Two-Scale Continuum Model for Simulation of Wormholes in Carbonate Acidization

Mohan K. R. Panga and Murtaza Ziauddin
Schlumberger, Sugar Land, TX 77478

Vemuri Balakotaiah
Dept. of Chemical Engineering, University of Houston, Houston, TX 77204

DOI 10.1002/aic.10574
Published online September 6, 2005 in Wiley InterScience (www.interscience.wiley.com).

A two-scale continuum model is developed to describe transport and reaction mechanisms in reactive dissolution of a porous medium, and used to study wormhole formation during acid stimulation of carbonate cores. The model accounts for pore level physics by coupling local pore-scale phenomena to macroscopic variables (Darcy velocity, pressure and reactant cup-mixing concentration) through structure-property relationships (permeability-porosity, average pore size-porosity, and so on), and the dependence of mass transfer and dispersion coefficients on evolving pore scale variables (average pore size and local Reynolds and Schmidt numbers). The gradients in concentration at the pore level caused by flow, species diffusion and chemical reaction are described using two concentration variables and a local mass-transfer coefficient. Numerical simulations of the model on a two-dimensional (2-D) domain show that the model captures the different types of dissolution patterns observed in the experiments. A qualitative criterion for wormhole formation is developed and it is given by $\Lambda \sim O(1)$, *where* $\Lambda = \sqrt{k_{eff} D_{eT}}/u_o$. *Here,* k_{eff} *is the effective volumetric dissolution rate constant,* D_{eT} *is the transverse dispersion coefficient, and* u_o *is the injection velocity. The model is used to examine the influence of the level of dispersion, the heterogeneities present in the core, reaction kinetics and mass transfer on wormhole formation. The model predictions are favorably compared to laboratory data.* © 2005 American Institute of Chemical Engineers *AIChE J,* 51: 3231–3248, 2005

Keywords: wormholes, carbonate acidizing, reactive dissolution, porous media

Introduction

Acid treatment of carbonate reservoirs is a widely practiced oil and gas well stimulation technique. The primary objective of this process is to increase the production rate by increasing permeability of the damaged zone near the wellbore region. The injected acid dissolves the material near the wellbore and creates flow channels that establish a good connectivity between the reservoir and the well. While dissolution increases permeability, the relative increase in permeability for a given amount of acid is observed to be a strong function of the injection conditions. At very low injection rates, acid is spent soon after it contacts the medium resulting in face dissolution. The penetration depth of the acid is restricted to a region very close to the wellbore. On the other hand, at very high injection rates, acid penetrates deep into the formation but the increase in permeability is not large because the acid reacts over a large region leading to uniform dissolution. At intermediate flow rates, long conductive channels known as wormholes are formed. These channels penetrate deep into the formation and

Correspondence concerning this article should be addressed to V. Balakotaiah at bala@uh.edu.

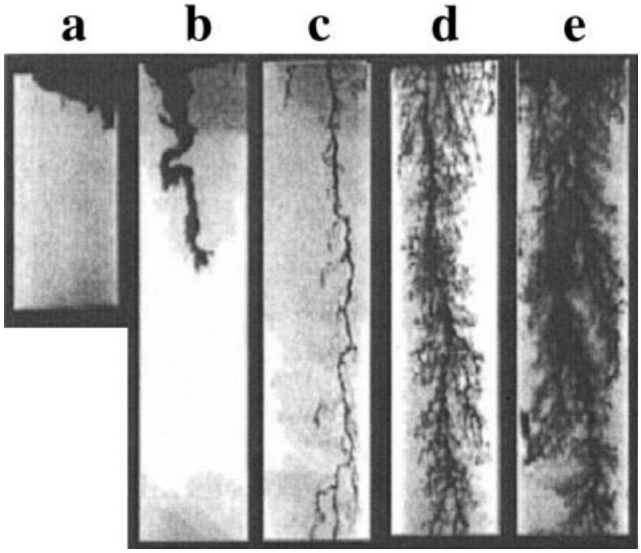

Figure 1. Typical dissolution patterns observed in carbonate acidizing: (a) face dissolution, Q = 0.04 cc/min, PV_{inj} = 43.1, (b) conical Q = 0.11 cc/min, PV_{inj} = 10, (c) wormhole Q = 1.05 cc/min, PV_{inj} = 0.8, (d) ramified Q = 10 cc/min, PV_{inj} = 2.1, and (e) uniform Q = 60 cc/min, PV_{inj} = 6.7.

Hydrochloric acid is used in these experiments and the acid injection rate is increased from (a) to (e) (Fredd and Fogler[15]). The cores are approximately 3.8 cm in dia. and 10.2 cm in length.

facilitate the flow of oil. Thus, for successful stimulation of a well it is required to produce wormholes with optimum density and penetrating deep into the formation. A detailed description of field practices for carbonate acidizing can be found in the literature.[1–4]

Several experimental studies have been conducted in the past to understand wormhole formation and to predict the conditions required for creating wormholes.[5–14] In those experiments, acid was injected into a core at different injection rates and the volume of acid required to break through the core, also known as breakthrough volume, was measured for each injection rate. A common observation in experimental studies is that dissolution creates patterns that are dependent on the injection rate. These dissolution patterns were broadly classified into three types: uniform, wormholing and face dissolution patterns corresponding to high, intermediate and low injection rates, respectively. Figure 1 shows typical dissolution patterns observed in experiments[15] on carbonate cores treated with HCl at different injection rates. It is also observed that wormholes form at an optimum injection rate, and because only a selective portion of the core is dissolved the volume required to stimulate the core is minimized (see Figure 2). Furthermore, the optimal conditions for wormhole formation were observed to depend on various factors such as acid/mineral reaction kinetics, diffusion coefficients of the acid species, concentration of acid, temperature, geometry of the system (linear/radial flow), and so on. Many theoretical studies have been conducted in the past to understand the phenomena of flow channeling associated with reactive dissolution in porous media, and to obtain an estimate of the optimum injection rate. However, the models developed thus far describe only a few aspects of the acidization process, and the coupling between reaction and transport mechanisms that plays a key role in reactive dissolution is not completely accounted for in these models. In this work, we present a two-scale continuum model that describes reaction and transport in a porous medium retaining the essential physics of dissolution. The model is used to investigate the influence of different factors on wormhole formation.

Literature Review

Wormhole formation during reactive dissolution of carbonates is a subject that has been actively studied in the last thirty years. To explain wormhole formation, numerous models, ranging from detailed pore-scale models (for example, network models) that account for reaction, transport and dissolution at the pore scale to single wormhole (tube) models that consider only the mechanisms occurring inside the wormholes, have been developed in the literature. In this section, a brief review of different models developed to study wormhole formation in carbonates is presented.

Relating the important dimensionless groups of the system to experimental observations is one of the approaches followed to model acidization process. For example, Fredd and Fogler[12,15] and Fredd[16] have reported the dependence of wormhole formation on the Damköhler number and predicted an optimum Damköhler number of 0.29 for different fluid/mineral systems. Daccord et al.[7,8,17] also used a dimensionless parameter based approach and coupled it with the concept of fractals to obtain the propagation rate of wormholes. The use of a few dimensionless groups to explain experimental observations is a difficult exercise because the actual number of parameters in the system is large and it is difficult to study wormholing phenomena systematically using this approach.

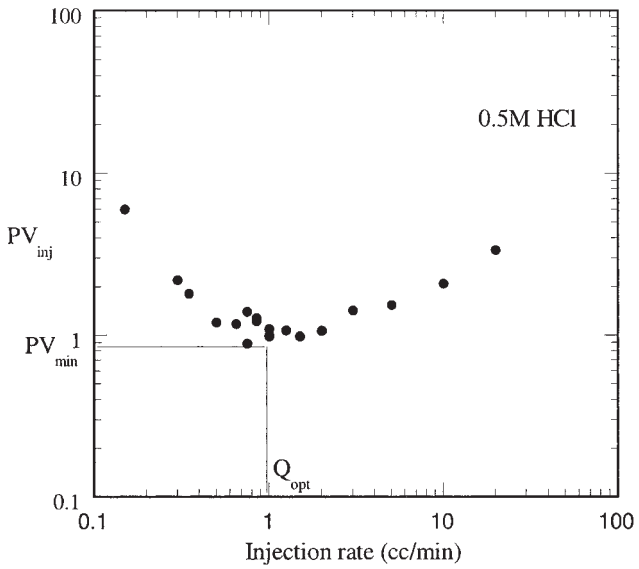

Figure 2. Typical breakthrough curve observed in acidization experiments.

The pore volume of acid (HCl, 22°C) required for breakthrough is high at very low and very high injection rates, and is minimum at optimum injection rate, Q_{opt}. The length and diameter of the cores are 10.2 cm and 3.8 cm, respectively. The initial porosities and permeabilities are in the range of 0.15–0.2 and 0.8–2 md, respectively.

In single wormhole models, a cylindrical tube represents the wormhole and the effects of fluid leakage, reaction kinetics, and so on, on wormhole propagation rate are investigated using these models.[10,14,18,19,20,21] One of the key results from the studies on single wormhole models is on the interaction of wormholes and competition between them. It has been reported[14,20] that the growth rates of multiple wormholes in a domain is dependent on the separation distance between them. Panga et al.[22] used a continuum model and made a similar observation in their numerical simulation of wormhole density. The simple structure of single wormhole models offers the advantage of studying reaction, diffusion and convection mechanisms inside the wormhole in detail; however, these models cannot be used to study wormhole initiation, the other dissolution patterns (face, ramified, and so on) observed in the experiments, and the effect of heterogeneities on wormhole formation.

Hoefner and Fogler,[9] Fredd and Fogler,[12] and Daccord et al.[17] have developed network models to describe reactive dissolution. Network models represent the porous medium as a network of tubes interconnected to each other at the nodes. The flow of acid inside these tubes is described using the Hagen-Poiseuille relationship for laminar flow. The acid reacts at the wall of the tube and dissolution is accounted for in terms of an increase in the tube radius. Network models predict the dissolution patterns and qualitative features of dissolution like the optimum flow rate observed in experiments. However, a core scale simulation of the network model is computationally very expensive.

An intermediate approach to describing reactive dissolution involves the use of averaged or continuum models. Unlike the network models that describe dissolution from the pore scale, and the models based on the assumption of existing wormholes, the averaged models describe dissolution at the Darcy scale. The Darcy scale model requires information on the pore scale processes, which are obtained from a pore scale model. The predictions of the pore scale model depend on the pore structure that changes with time due to dissolution. Obtaining detailed pore structure of a core and approximating its change during dissolution is very difficult and is one of the disadvantages of using a Darcy scale model. However, by using different pore scale models that are representative of the core, the sensitivity of the results obtained from Darcy scale models can be studied. Averaged models for carbonate acidization have been developed by Liu et al.[23] Chen et al.[24,25] and Golfier et al.[26] These models were shown to capture qualitative and some quantitative features of dissolution. The model developed by Liu et al. and Chen et al. does not consider the effect of mass transfer on the reaction rate and is valid only in the kinetic regime, while the model developed by Golfier et al. is valid only in the mass-transfer controlled regime (to be defined later). This work presents a continuum model that captures both the extremes of reaction (kinetic and mass transfer controlled) simultaneously by using two concentration variables and a mass-transfer coefficient. This allows the description of a wide range of acids as demonstrated later. The model proposed here is similar to the widely used two-phase models of catalytic reactors,[27] the main difference being coupling of the flow, dissolution/reaction and pore scale mass-transfer processes.

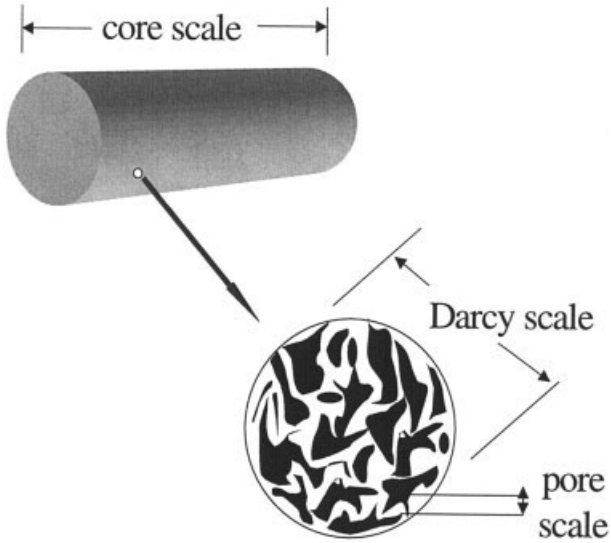

Figure 3. Different length scales used in the model.

Model for Carbonate Dissolution

Reaction between a carbonate porous medium and acid leads to complete dissolution of the medium, thereby increasing the permeability to a large value. At very low injection rates in a homogeneous medium, this would give rise to a planar reaction/dissolution front where the medium behind the front is completely dissolved and the medium ahead of the front is not dissolved. However, the presence of natural heterogeneities in the medium leads to an uneven increase in permeability along the front leading to regions of high and low permeabilities. The high permeability regions attract more acid, which further dissolves the medium creating channels that travel ahead of the front. Thus, adverse mobility ($=K/\mu$, where K is the permeability and μ is the viscosity of the fluid) arising because of differences in the permeabilities of the dissolved and undissolved medium and heterogeneity are required for channel formation. This reaction-driven instability has been studied using linear and weakly nonlinear stability analyses by some authors.[28,29,30,31] This instability is similar to the viscous fingering instability where adverse mobility arises due to a difference in viscosities of the displacing and displaced fluids.[32]

The shape (wormhole, conical, and so on) of the channels is, however, dependent on the relative magnitudes of convection and dispersion in the medium. For example, when transverse dispersion is more dominant than convective transport, reaction leads to conical and face dissolution patterns. On the other hand, when convective transport is more dominant, the concentration of acid is more uniform in the domain leading to a uniform dissolution pattern. The model presented here describes the phenomena of reactive dissolution as a coupling between processes occurring at *two scales,* namely the Darcy scale and the pore scale. Different length scales are shown in Figure 3. In the following subsections, these two parts of the model are discussed.

Darcy scale model

The Darcy scale model equations are given by

$$\mathbf{U} = -\frac{1}{\mu}\mathbf{K}\cdot\nabla P \tag{1}$$

$$\frac{\partial \varepsilon}{\partial t'} + \nabla\cdot\mathbf{U} = 0 \tag{2}$$

$$\frac{\partial(\varepsilon C_f)}{\partial t'} + \nabla\cdot(\mathbf{U}C_f) = \nabla\cdot(\varepsilon\mathbf{D}_e\cdot\nabla C_f) - k_c a_v(C_f - C_s) \tag{3}$$

$$k_c(C_f - C_s) = R(C_s) \tag{4}$$

$$\frac{\partial \varepsilon}{\partial t'} = \frac{R(C_s)a_v\alpha}{\rho_s} \tag{5}$$

Here $\mathbf{U} = (U, V, W)$ is the Darcy velocity vector, $\mathbf{K}$ is the permeability tensor, P is the pressure, ε is the porosity, C_f is the cup-mixing concentration of the acid in the fluid phase, C_s is the concentration of the acid at the fluid-solid interface, $\mathbf{D}_e$ is the effective dispersion tensor, k_c is the local mass-transfer coefficient, a_v is the interfacial area available for reaction per unit volume of the medium, ρ_s is the density of the solid phase and α is the dissolving power of the acid, defined as grams of solid dissolved per mole of acid reacted. The reaction kinetics is represented by $R(C_s)$. For a first-order reaction $R(C_s)$ reduces to k_sC_s where k_s is the surface reaction rate constant (having the units of velocity).

Equation 3 gives a Darcy scale description of the transport of the acid species. The first three terms in the equation represent accumulation, convection and dispersion of the acid, respectively. The fourth term describes the transfer of acid species from the fluid phase to the fluid-solid interface and its role is discussed later in this section. The velocity field $\mathbf{U}$ in the convection term is obtained from Darcy's law (Eq. 1) relating velocity to the permeability field $\mathbf{K}$ and the gradient of pressure. The first term in the continuity Eq. 2 accounts for the effect of local volume change during dissolution on the flow field. While deriving the continuity equation, it is assumed that the dissolution process does not change the density of the fluid phase significantly.

The transfer term in the species balance Eq. 3 describes the depletion of the reactant at the Darcy scale due to reaction. An accurate estimation of this term depends on the description of transport and reaction mechanisms inside the pores. In the absence of reaction, concentration of the acid species is uniform inside the pores. Reaction at the solid-fluid interface gives rise to concentration gradients in the fluid phase inside the pores. The magnitude of these gradients depends on the relative rate of mass transfer from the fluid phase to the fluid-solid interface and reaction at the interface. If the reaction rate is very slow compared to the mass-transfer rate, the concentration gradients are negligible. In this case, the reaction is considered to be in the *kinetically controlled regime,* and a single concentration variable is sufficient to describe this situation. However, if the reaction is very fast compared to the mass transfer, steep gradients develop inside the pores. This regime of reaction is known as the *mass-transfer controlled regime.* To account for the gradients developed due to mass transfer control requires the solution of a differential equation describing diffusion and reaction mechanisms inside each of the pores. Since this is impractical, we use two concentration variables C_s and C_f, for the concentration of the acid at the fluid-solid interface and in the fluid phase respectively, and capture the information contained in the local concentration gradients as a difference between the two variables using the concept of a local mass-transfer coefficient (Eq. 4).

Equation 4 balances the amount of reactant transferred to the surface to the amount reacted. For the case of first order kinetics, $R(C_s) = k_sC_s$, Eq. 4 can be simplified to

$$C_s = \frac{C_f}{\left(1 + \frac{k_s}{k_c}\right)} \tag{6}$$

In the kinetically controlled regime ($k_s \ll k_c$), the concentration at the fluid-solid interface is approximately equal to the concentration of the fluid phase ($C_s \approx C_f$). In the mass transfer controlled regime ($k_s \gg k_c$), the value of concentration at the fluid-solid interface is very small ($C_s \approx 0$). Since the rate constant is fixed for a given acid, the magnitude of the ratio k_s/k_c is determined by the local mass-transfer coefficient k_c, which is a function of the pore geometry, the reaction rate and the local hydrodynamics. Due to dissolution and heterogeneity in the medium, the ratio k_s/k_c is not a constant in the medium but varies with space and time which can lead to a situation where different locations in the medium experience different regimes of reaction. To describe such a situation it is essential to account for both kinetic and mass transfer controlled regimes in the model. Equation 5 describes the evolution of porosity in the domain due to reaction.

To complete the model (Eqs. 1–5), information on the permeability tensor $\mathbf{K}$, dispersion tensor $\mathbf{D}_e$, mass-transfer coefficient k_c, and interfacial area a_v is required. These quantities depend on the pore structure and are inputs to the Darcy scale model from the pore scale model. Instead of calculating these quantities from a detailed pore scale model taking into consideration the actual pore structure, we use structure-property relations that relate permeability, interfacial area and average pore radius of the pore scale model to its porosity. However, if a detailed calculation including the pore structure can be made, then the quantities $\mathbf{K}$, $\mathbf{D}_e$, k_c, and a_v obtained from such a calculation can be used as inputs from the pore scale model to the Darcy scale model.

Pore scale model

(a) Structure-Property Relations. Dissolution changes the structure of the porous medium continuously, thus, making it difficult to correlate the changes in local permeability to porosity during acidization. The results obtained from averaged models, which use these correlations, are subject to quantitative errors arising from the use of a bad correlation between the structure and property of the medium, although the qualitative trends predicted may be correct. Since a definitive way of relating the change in the properties of the medium to the change in structure during dissolution does not exist, we use

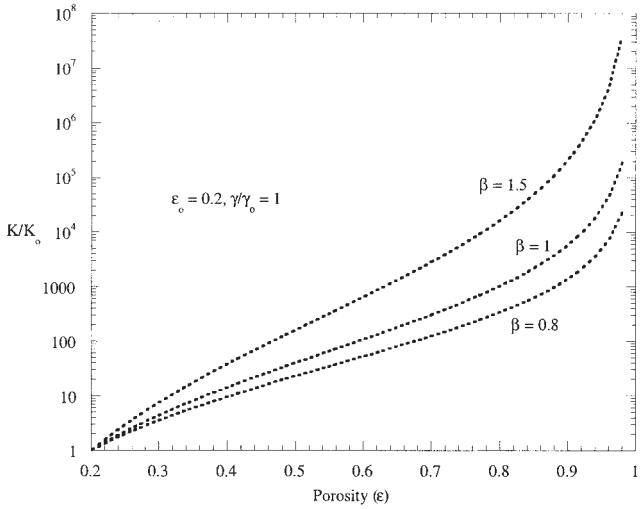

Figure 4. Variation of permeability with porosity for different values of β.

semiempirical relations that relate the properties to local porosity. The relative increase in permeability, pore radius and interfacial area with respect to their initial values are related to porosity in the following manner

$$\frac{K}{K_o} = \frac{\varepsilon}{\varepsilon_o}\left(\frac{\varepsilon(1-\varepsilon_o)}{\varepsilon_o(1-\varepsilon)}\right)^{2\beta} \tag{7}$$

$$\frac{r_p}{r_o} = \sqrt{\frac{K\varepsilon_o}{K_o\varepsilon}} \tag{8}$$

and

$$\frac{a_v}{a_o} = \frac{\varepsilon r_o}{\varepsilon_o r_p} \tag{9}$$

Here K_o, r_o and a_o are the initial values of permeability, average pore radius and interfacial area, respectively. Notice that, for $\beta = 1$ the structure-property relation for permeability evolution reduces to the well-known Carman-Kozeny correlation $K \propto \varepsilon^3/(1-\varepsilon)^2$ relating permeability to the porosity of the medium. The parameter β is introduced into Eq. 7 to extend the relation to a dissolving medium. Figure 4 shows a typical plot of permeability versus porosity for different values of the parameter β. In addition, the effect of structure-property relations on breakthrough time has also been tested by using different correlations (in a later section). The model yields better results if structure-property correlations that are developed for a particular system of interest are used. Note that, in the earlier relations permeability, which is a tensor, is reduced to a scalar for the pore scale model. In the case of anisotropic permeability, extra relations for the permeability of the pore scale model are needed to complete the model.

(b) Mass-Transfer Coefficient. Transport of the acid species from the fluid phase to the fluid-solid interface inside the pores is quantified by the mass-transfer coefficient (k_c). It plays an important role in characterizing dissolution phenomena because the mass-transfer coefficient determines the regime of reaction for a given acid (Eq. 6). The mass-transfer coefficient depends on the local pore structure, reaction rate and local velocity of the fluid. Gupta and Balakotaiah[33] and Balakotaiah and West[34] investigate the contribution of each of these factors to the local mass-transfer coefficient in detail. For developing flow inside a straight pore of arbitrary cross section, it is shown[34] that a good approximation to the Sherwood number, the dimensionless mass-transfer coefficient, is given by

$$Sh = \frac{2k_c r_p}{D_m} = Sh_\infty + 0.35\left(\frac{d_h}{x}\right)^{0.5} \mathrm{Re}_p^{1/2} Sc^{1/3} \tag{10}$$

where k_c is the mass-transfer coefficient, r_p is the pore radius and D_m is molecular diffusivity, Sh_∞ is the asymptotic Sherwood number for the pore, Re_p is the pore Reynolds number, d_h is the pore hydraulic diameter, x is the distance from the pore inlet and Sc is the Schmidt number ($Sc = \nu/D_m$; where ν is the kinematic viscosity of the fluid). Assuming that the length of a pore is typically a few pore diameters, the average mass-transfer coefficient can be obtained by integrating the above expression over a pore length, which gives

$$Sh = Sh_\infty + b\ \mathrm{Re}_p^{1/2} Sc^{1/3} \tag{11}$$

where the constants Sh_∞ and b (=0.7/m$^{1/2}$, m = pore length to diameter ratio) depend on the structure of the porous medium (pore cross sectional shape and pore length to hydraulic diameter ratio). Equation 11 is of the same general form as the Frossling correlation used extensively in correlating mass-transfer coefficients in packed-beds. (For a packed bed of spheres, $Sh_\infty = 2$ and $b = 0.6$. This value of b is close to the theoretical value of 0.7 predicted by Eq. 11 for $m = 1$.)

The two terms on the righthand side of Eq. 11 are contributions to the Sherwood number due to diffusion and convection of the acid species, respectively. While the diffusive part, Sh_∞ depends on the pore geometry, the convective part is a function of the local velocity. The asymptotic Sherwood number for pores with cross-sectional shape of square, triangle and circle are 2.98, 2.50 and 3.66, respectively.[34] Since the value of asymptotic Sherwood number is a weak function of the pore cross-sectional geometry, we use a typical value of 3.0 in our calculations. The convective part depends on the pore Reynolds number and the Schmidt number. For liquids, the typical value of Schmidt number is around one thousand and assuming a value of 0.7 for b, the approximate magnitude of the convective part of the Sherwood number from Eq. 11 is 7 $\mathrm{Re}_p^{1/2}$. The pore Reynolds numbers are very small due to the small pore radius, and the low injection velocities of the acid, making the contribution of the convective part negligible during the initial stages of dissolution. As dissolution proceeds, the pore radius and the local velocity increase, making the convective contribution significant. (Remark: For typical values cited above, the two contributions are equal when 7 $\mathrm{Re}_p^{1/2} \approx 3$ or $\mathrm{Re}_p \approx 0.2$.) However, the effect of this convective mass transfer on acid consumption may not be significant because of the extremely low interfacial area in the high porosity regions where convection is dominant. The effect of reaction rate on the mass-transfer coefficient is observed to be weak.[34] For example, the asymptotic Sherwood number varies from 48/11

(=4.36) to 3.66 in the case of a very slow reaction to a very fast reaction.

(c) Fluid Phase Dispersion Coefficients. For homogeneous, isotropic porous media, the dispersion tensor is characterized by two independent components, namely, the longitudinal, D_{eX} and transverse, D_{eT}, dispersion coefficients. In the absence of flow, dispersion of a solute occurs only due to molecular diffusion and $D_{eX} = D_{eT} = \alpha_{os} D_m$, where D_m is the molecular diffusion coefficient and α_{os} is a constant that depends on the structure of the porous medium (for example, tortuosity or connectivity between the pores). With flow, the dispersion tensor depends on the morphology of the porous medium, as well as the pore level flow and fluid properties. The relative importance of convective to diffusive transport at the pore level is characterized by the Peclet number in the pore, defined by

$$Pe_p = \frac{|\mathbf{U}| d_h}{\varepsilon D_m} \tag{12}$$

where $|\mathbf{U}|$ is the magnitude of the Darcy velocity, and d_h is the pore hydraulic diameter. For a well-connected pore network, random walk models and analogy with packed beds may be used to show that

$$D_X = \frac{D_{eX}}{D_m} = \alpha_{os} + \lambda_X Pe_p \tag{13}$$

and

$$D_T = \frac{D_{eT}}{D_m} = \alpha_{os} + \lambda_T Pe_p \tag{14}$$

where λ_X and λ_T are numerical coefficients that depend on the structure of the medium ($\lambda_X \approx 0.5$, $\lambda_T \approx 0.1$ for packed-bed of spheres). Other correlations used for D_{eX}, are of the form

$$\frac{D_{eX}}{D_m} = \alpha_{os} + \frac{1}{6} Pe_p \ln\left(\frac{3Pe_p}{2}\right) \tag{15}$$

and

$$\frac{D_{eX}}{D_m} = \alpha_{os} + \lambda Pe_p^2. \tag{16}$$

Equation 16 is based on Taylor-Aris theory, and it is normally used when the connectivity between the pores is very low. These as well as the other correlations in the literature predict that both the longitudinal and transverse dispersion coefficients increase with the Peclet number.

Table 1 shows typical values of pore Peclet numbers calculated, based on the core experiments (permeability of the cores is approximately 1 mD) of Fredd and Fogler.[12] The injection velocities of the acid (0.5 M HCl) are varied between 0.14 cm/s and 1.4×10^{-4} cm/s, where 0.14 cm/s corresponds to the uniform dissolution regime and 1.4×10^{-4} cm/s corresponds to the face dissolution regime. The values of pore diameter, molecular diffusion and porosity used in the calculations are

Table 1. Pore Level Peclet Numbers at Different Injection Rates

Regime	Injection Velocity (cm/s)	Pe_p
Face	1.4×10^{-4}	7×10^{-4}
Wormhole	1.4×10^{-3}	7×10^{-3}
Uniform	0.14	0.7

0.1 μm, 2×10^{-5} cm^2/s and 0.2, respectively. It appears from the low values of pore level Peclet number in the face dissolution regime that dispersion in this regime is primarily due to molecular diffusion. The Peclet number is close to order unity in the uniform dissolution regime showing that both molecular and convective contributions are of equal order. In the numerical simulations presented later, it is observed that the dispersion term in Eq. 3 does not play a significant role at high injection rates (uniform dissolution regime) where convection is the dominant mechanism. As a result, the form of the convective part of the dispersion ($\lambda_X Pe_p$, $Pe_p \ln(3Pe/2)$, and so on), which becomes important in the uniform dissolution regime, may not affect the breakthrough times at low permeabilities. In this work, we use the dispersion relations given by Eqs. 13 and 14 to complete the averaged model. (Remark: As a first approximation, we have assumed that the mass transfer coefficient to be the same in the axial and transverse directions. However, as in the case of the dispersion coefficient, the convective contribution to mass transfer could be different in the flow and transverse directions. This can be accounted for by replacing the scalar k_c by the transfer matrix (a tensor). We do not pursue this here.)

Dimensionless Model Equations and Limiting Cases

The model equations for first-order irreversible kinetics are made dimensionless for the case of constant injection rate at the inlet boundary by defining the following dimensionless variables

$$x = \frac{x'}{L}, \quad y = \frac{y'}{L}, \quad z = \frac{z'}{L}, \quad \mathbf{u} = \frac{\mathbf{U}}{u_o}, \quad t = \frac{t'}{(L/u_o)},$$

$$r = \frac{r_p}{r_o}, \quad A_v = \frac{a_v}{a_o}, \quad \kappa = \frac{K}{K_o},$$

$$c_f = \frac{C_f}{C_o}, \quad c_s = \frac{C_s}{C_o}, \quad p = \frac{P - P_e}{\dfrac{\mu u_o L}{K_o}}$$

$$\phi^2 = \frac{2k_s r_o}{D_m}, \quad Da = \frac{k_s a_o L}{u_o}, \quad N_{ac} = \frac{\alpha C_o}{\rho_s},$$

$$Pe_L = \frac{u_o L}{D_m}, \quad \eta = \frac{2r_o}{L}, \quad \alpha_o = \frac{H}{L}$$

where L is the characteristic length scale in the (flow) x' direction, H is the height of the domain, u_o is the inlet velocity, C_o is the inlet concentration of the acid and P_e is the pressure at the exit boundary of the domain. The initial values of permeability, interfacial area and average pore radius are rep-

resented by K_o, a_o and r_o, respectively. The parameters obtained after making the equations dimensionless are the Thiele modulus ϕ^2, the Damköhler number Da, the acid capacity number N_{ac}, the axial Peclet number Pe_L, aspect ratio α_o, and η. The Thiele modulus (ϕ^2) is defined as the ratio of diffusion time to reaction time based on the initial pore size and the Damköhler number (Da) is defined as the ratio of convective time to reaction time based on the length scale of the core. The acid capacity number (N_{ac}) is defined as the volume of solid dissolved per unit volume of the acid, and the axial Peclet number Pe_L is the ratio of axial diffusion time to convection time. Notice that in the above parameters, inlet velocity u_o appears in two parameters Da and Pe_L. To eliminate inlet velocity from one of the parameters, so that the variable of interest, that is, injection velocity, appears in only one dimensionless parameter (Da) we introduce a macroscopic Thiele modulus Φ^2 which is defined as $\Phi^2 = k_s a_o L^2/D_m = DaPe_L$. The macroscopic Thiele modulus is a core scale equivalent of the pore scale Thiele modulus (ϕ^2), and is independent of injection velocity. The dimensionless equations in the two-dimensional (2-D) case are given by

$$(u, v) = \left(-\kappa \frac{\partial p}{\partial x}, -\kappa \frac{\partial p}{\partial y} \right) \tag{17}$$

$$\frac{\partial \varepsilon}{\partial t} + \frac{\partial u}{\partial x} + \frac{\partial v}{\partial y} = 0 \tag{18}$$

$$\frac{\partial(\varepsilon c_f)}{\partial t} + \frac{\partial(u c_f)}{\partial x} + \frac{\partial(v c_f)}{\partial y} = -\frac{DaA_v c_f}{\left(1 + \frac{\phi^2 r}{Sh}\right)} + \frac{\partial}{\partial x}\left[\left\{\frac{\alpha_{os}\varepsilon Da}{\Phi^2} + \lambda_x |\mathbf{u}| r\eta\right\}\frac{\partial c_f}{\partial x}\right] + \frac{\partial}{\partial y}\left[\left\{\frac{\alpha_{os}\varepsilon Da}{\Phi^2} + \lambda_T |\mathbf{u}| r\eta\right\}\frac{\partial c_f}{\partial y}\right] \tag{19}$$

$$\frac{\partial \varepsilon}{\partial t} = \frac{DaN_{ac}A_v c_f}{\left(1 + \frac{\phi^2 r}{Sh}\right)} \tag{20}$$

The boundary and initial conditions used to solve the system of equations are given below

$$-\kappa \frac{\partial p}{\partial x} = 1 \ @ \ x = 0 \tag{21}$$

$$p = 0 \ @ \ x = 1 \tag{22}$$

$$-\kappa \frac{\delta p}{\delta y} = 0 \ @ \ y = 0, \ \alpha_0 \tag{23}$$

$$c_f = 1 \ @ \ x = 0 \tag{24}$$

$$\frac{\partial c_f}{\partial x} = 0 \ @ \ x = 1 \tag{25}$$

$$\frac{\partial c_f}{\partial y} = 0 \ @ \ y = 0 \quad \text{and} \quad y = \alpha_o \tag{26}$$

$$c_f = 0 \ @ \ t = 0 \tag{27}$$

$$\varepsilon(x, y, a, l) = \varepsilon_0 + \hat{f}(a,l) \ @ \ t = 0 \tag{28}$$

A constant injection rate boundary condition given by Eq. 21 is imposed at the inlet of the domain and the fluid is contained in the domain by imposing zero flux boundary conditions (Eq. 23) on the lateral sides of the domain. The boundary conditions for the transport of acid species are given by Eqs. 24–26. It is assumed that there is no acid present in the domain at time $t = 0$. To simulate wormhole formation numerically, it is necessary to have heterogeneity in the domain which is introduced by assigning different porosity values to different grid cells in the domain according to Eq. 28. The porosity values are generated by adding a random number ($\hat{f}$) uniformly distributed in the interval $[-\Delta\varepsilon_o, \Delta\varepsilon_o]$ to the mean value of porosity ε_o. The quantity a defined as $a = \Delta\varepsilon_o/\varepsilon_o$ is the magnitude of heterogeneity, and the parameter l is the dimensionless length scale of heterogeneity which is scaled using the pore diameter that is, $l = L_h/(2r_o) = L_h/(\eta L)$, where L_h is equal to the length scale of the heterogeneity. Unless stated otherwise, L_h is taken as the size of the grid in numerical simulations.

The earlier system of equations can be reduced to a simple form at very high or very low injection rates to obtain analytical relations for pore volumes required to breakthrough. Face dissolution occurs at very low injection rates where the acid is consumed as soon as it comes in contact with the medium. As a result, the acid has to dissolve the entire medium before it reaches the exit for breakthrough. The stoichiometric pore volume of acid required to dissolve the whole medium is given by

$$PV_{FaceD} = \frac{\rho_s(1 - \varepsilon_o)}{\alpha C_o \varepsilon_o} = \frac{(1 - \varepsilon_o)}{N_{ac}\varepsilon_o} \tag{29}$$

where C_o is the inlet concentration of the acid, and ε_o is the initial porosity of the medium. At very high injection rates, the residence time of the acid is very small compared to the reaction time and most of the acid escapes the medium without reacting (Remark: It is difficult to reach this asymptote experimentally). Because the conversion of the acid is low, the concentration in the medium could be approximated as the inlet concentration. Under these assumptions the model could be reduced to

$$\frac{\partial \varepsilon}{\partial t} = \frac{k_s C_o a_v \alpha}{\rho_s\left(1 + \frac{\phi^2 r}{Sh}\right)} \tag{30}$$

Denoting the final porosity required to achieve a fixed increase in the permeability by ε_f (this could be calculated from Eq. 7), the earlier equation can be integrated for the breakthrough time

$$t_{bth} = \frac{\rho_s}{k_s C_o \alpha} \int_{\varepsilon_o}^{\varepsilon_f} \frac{\left(1 + \frac{\phi^2 r}{Sh}\right)}{a_v} d\varepsilon \tag{31}$$

Thus, the pore volume of acid required for breakthrough at high injection rates is given by

$$PV_{UniformD} = \frac{t_{bth} u_o}{\varepsilon_o L} = \frac{\rho_s u_o}{k_s C_o \alpha a_o \varepsilon_o L} \int_{\varepsilon_o}^{\varepsilon_f} \frac{\left(1 + \frac{\phi^2 r}{Sh}\right)}{A_v} d\varepsilon$$

$$= \frac{1}{DaN_{ac}\varepsilon_o} \int_{\varepsilon_o}^{\varepsilon_f} \frac{\left(1 + \frac{\phi^2 r}{Sh}\right)}{A_v} d\varepsilon$$

The breakthrough volume increases with increasing velocity.

To achieve a fixed increase in the permeability, a large volume of acid is required in the uniform dissolution regime where the acid escapes the medium after partial reaction. Similarly, in the face dissolution regime a large volume of acid is required to dissolve the entire medium. In the wormholing regime only a part of the medium is dissolved to increase the permeability by a given factor, thus, decreasing the volume of acid required than that in the face and uniform dissolution regimes. Since spatial gradients do not appear in the asymptotic limits (Eq. 29 and Eq. 30) the results obtained from 1-D, 2-D and 3-D models for pore volume of acid required to achieve breakthrough should be independent of the dimension of the model at very low and very high injection rates for a given acid. However, optimum injection rate and minimum volume of acid that arise due to channeling are dependent on the dimension of the model. The pore volume required for breakthrough vs the injection rate is shown in Figure 5 for 1-D, 2-D and 3-D models.

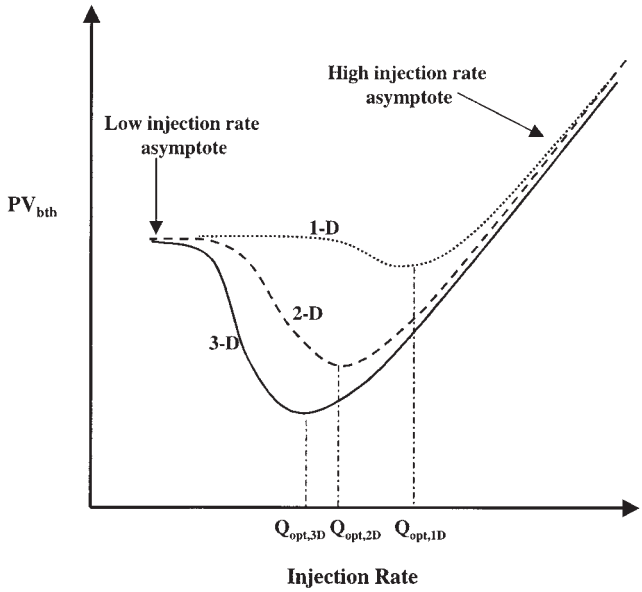

Figure 5. Qualitative trends in breakthrough curves for 1-D, 2-D and 3-D models.

The optimum injection rate and the minimum pore volume decrease from 1-D to 3-D due to channeling.

2-D Dissolution Patterns

In this section, numerical simulations illustrating the effect of heterogeneity, different transport mechanisms and reaction kinetics on dissolution patterns are presented. The model is simulated on a rectangular 2-D porous medium of dimensions 2 cm × 5 cm ($\alpha_o = 0.4$). Acid is injected at a constant rate at the inlet boundary of the domain, and it is contained in the domain by imposing a zero flux boundary condition on the lateral sides of the domain. The simulation is stopped once the acid breaks through the exit boundary of the domain. Here, breakthrough is defined as decrease in the pressure drop by a factor of 100 (or increase in the overall permeability of the medium by 100) from the initial pressure drop. The numerical scheme used to solve the governing equations is described in Appendix-A. The value of initial porosity in the domain is 0.2. The effect of injection rate on the dissolution patterns is studied by varying the Damköhler number (Da), which is inversely proportional to the velocity. In addition to the dimensionless injection rate (Da), the other important dimensionless parameters in the model are ϕ^2, N_{ac}, Φ^2, a and l. The effect of these parameters on wormhole formation is investigated.

(a) Magnitude of Heterogeneity. As discussed earlier, heterogeneity is an important factor that promotes pattern formation during reactive dissolution. Without heterogeneity, the reaction/dissolution fronts would be uniform despite an adverse mobility ratio between the dissolved and undissolved media. In a real porous medium, the presence of natural heterogeneities triggers instability leading to different dissolution patterns. To simulate these patterns numerically, it is necessary to introduce heterogeneity into the model. Heterogeneity could be introduced in the model as a perturbation in concentration at the inlet boundary of the domain or as a perturbation in the initial porosity or permeability field in the domain. In the present model, heterogeneity is introduced into the domain as a random fluctuation of initial porosity values about the mean value of porosity as given by Eq. 28. The two important parameters defining heterogeneity are the magnitude of heterogeneity a, and the dimensionless length scale l. The effect of these parameters on wormhole formation is investigated in this, and the following subsections.

The influence of the magnitude of heterogeneity (a) is studied by maintaining the length scale of heterogeneity constant (which is the grid size) and varying the magnitude from a small to a large value. Figures 6a–6e show the porosity profiles of numerically simulated dissolution patterns for different Damköhler numbers on a domain with a large magnitude of heterogeneity in initial porosity distribution. The fluctuations ($\hat{f}$) in porosity ($\varepsilon = 0.2 + \hat{f}$) are uniformly distributed in the interval $[-0.15, 0.15]$ ($a = 0.75$). Figures 6f–6j show the porosity profiles for the same Damköhler numbers used in Figures 6a–6e, but with a small magnitude of heterogeneity in the initial porosity distribution. The fluctuations ($\hat{f}$) in porosity ($\varepsilon = 0.2 + \hat{f}$) for this case are distributed in the interval $[-0.05, 0.05]$ ($a = 0.25$). It could be observed from the figures that wormholes do not exhibit branching when the magnitude of heterogeneity is decreased. This observation suggests that branching of wormholes observed in carbonate cores

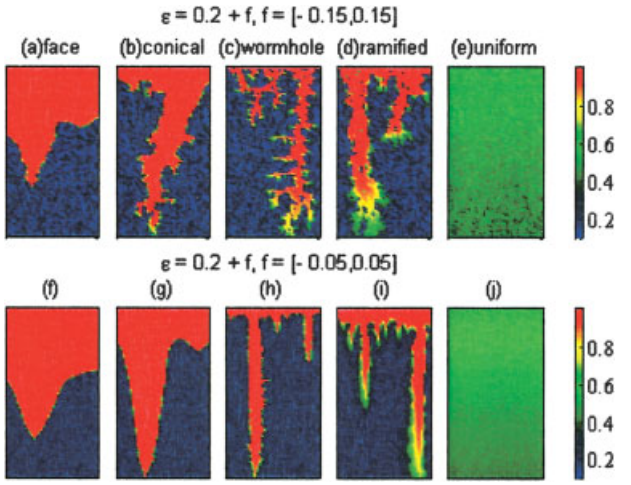

Figure 6. Porosity profiles at different Damköhler numbers with fluctuations in initial porosity distribution in the interval [−0.15, 0.15] are shown in Figures a–e.

Figures f–j show porosity profiles for the same Damköhler numbers as used in Figures a–e, but for fluctuations in the interval [−0.05, 0.05]. The values of Damköhler numbers for different patterns are: (a) $Da = 3 \times 10^4$ ($\Lambda_o = 30$), (b) $Da = 10^4$ ($\Lambda_o = 10$), (c) $Da = 500$ ($\Lambda_o = 0.5$), (d) $Da = 40$ ($\Lambda_o = 0.04$), and (e) $Da = 1$ ($\Lambda_o = 0.001$). The values of parameter Λ_o are reported for later use. The values of other parameters fixed in the model are $\Phi^2 = 10^6$, $\phi^2 = 0.07$, $N_{ac} = 0.1$, $\alpha_o = 0.4$.

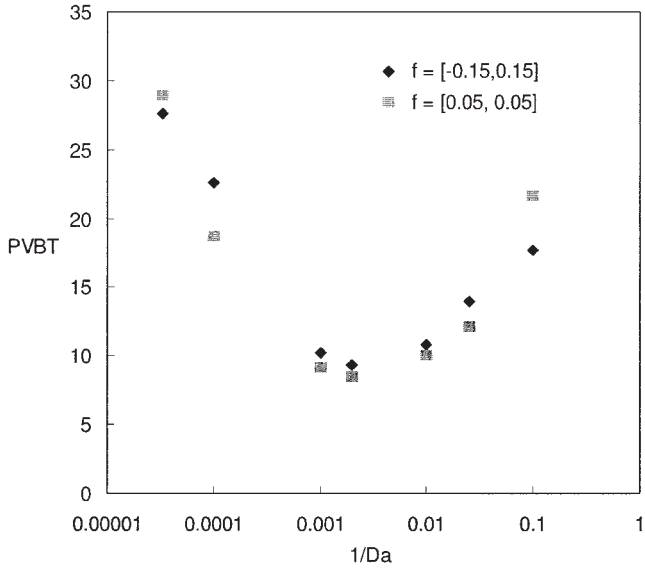

Figure 7. Breakthrough curves for different magnitudes of heterogeneity used in Figure 6.

The volume of acid required to breakthrough the core at different injection rates is not a strong function of the magnitude of heterogeneity.

could be a result of a wide variation in magnitude of heterogeneities present in the core. Figures 6a–6j show that at very large Damköhler numbers (low injection rates), the acid reacts soon after it contacts the medium resulting in face dissolution, and at low values of Damköhler number (high injection rates), acid produces a uniform dissolution pattern. Wormholing patterns are created near intermediate/optimum values of the Damköhler number. While changing the magnitude of heterogeneity changes the structure of the wormholes, an important observation to be made here is that the type of dissolution pattern (wormhole, conical, and so on) remains the same at a given Damköhler number for different magnitudes of heterogeneity. Thus, heterogeneity is required to trigger the instability and its magnitude determines wormhole structure, but the type of dissolution pattern formed is governed by the transport and reaction mechanisms. Figure 7 shows the pore volume of acid required to breakthrough the core at different injection rates with different levels of heterogeneity for the porosity profiles shown in Figure 6. The curves show a minimum at intermediate injection rates because of wormhole formation. It could be observed from the breakthrough curves that the minimum pore volume/breakthrough time and optimum injection rate (Damköhler number) are approximately the same for both levels of heterogeneity.

The second parameter related to heterogeneity that is introduced in the model is the length scale of heterogeneity l. The effect of this parameter on wormhole structure is dependent on the relative magnitudes of convection, reaction and dispersion levels in the system. The role of this parameter on wormhole formation is thus discussed after investigating the effects of convection, reaction and transverse dispersion in the system.

(b) Convection and Transverse Dispersion. In the previous subsection, it was shown that the magnitude of heterogeneity affects wormhole structure but its influence on optimum Damköhler number is not significant. The dissolution pattern produced is observed to depend on the relative magnitudes of convection, reaction and dispersion in the system. Because of the large variation in injection velocities (over three orders of magnitude) in core experiments, different transport mechanisms become important at different injection velocities, each leading to a different dissolution pattern. For example, at high injection velocities convection is more dominant than dispersion and it leads to uniform dissolution, whereas at low injection velocities dispersion is more dominant than convection leading to face dissolution. A balance between convection, reaction and dispersion levels in the system produces worm-

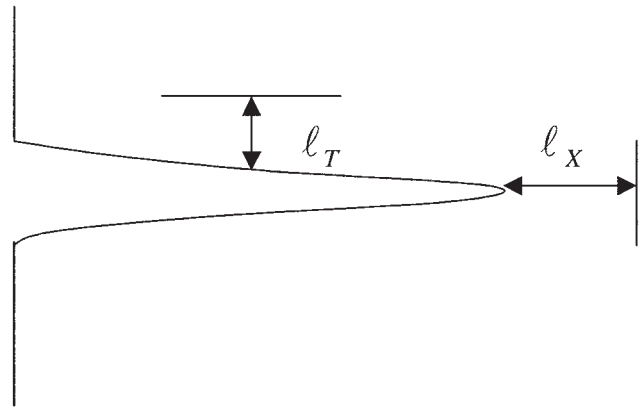

Figure 8. Reaction front thickness in the longitudinal and transverse directions to the mean flow.

The front thickness is represented by l_X in the flow direction and l_T in the transverse direction.

holes. In this subsection, a qualitative analysis is first presented to identify the important parameters that determine the optimum velocity for wormhole formation and the minimum pore volume of acid. Numerical simulations are performed to show the relevance of these parameters.

Consider a channel in a porous medium (see Figure 8) created because of reactive dissolution of the medium. The injected acid reacts in the medium ahead of the tip and adjacent to the walls of the channel and increases the length, as well as the width of the channel. If the growth of the channel in the direction of flow is faster than its growth in the transverse direction then the resulting shape of the channel is thin and is called a wormhole. On the other hand, if the growth is much faster in the transverse direction compared to the flow direction then the channel assumes a conical shape. To find the relative growth in each direction, it is necessary to identify the dominant mechanisms by which acid is transported in the direction of flow and transverse to the flow. Because of a relatively large pressure gradient in the flow direction, the main mode of transport in this direction is convection. In the transverse direction, convective velocities are small and the main mode of transport is through dispersion. If we denote the length of the front in the medium ahead of the tip where the acid is consumed by l_X, and the front length in the transverse direction by l_T, a qualitative criterion for different dissolution patterns can be given by

$$\frac{l_T}{l_X} \gg O(1) \Rightarrow \text{Face dissolution} \tag{32}$$

$$\frac{l_T}{l_X} \sim 0.1 \text{ to } 1 \Rightarrow \text{Wormhole} \tag{33}$$

and

$$\frac{l_T}{l_X} \ll O(1) \Rightarrow \text{uniform dissolution} \tag{34}$$

An approximate magnitude of l_X can be obtained from the convection-reaction equation

$$u_{tip} \frac{\partial C_f}{\partial x'} = -k_{eff} C_f \tag{35}$$

where u_{tip} is the velocity of the fluid at the tip of the wormhole and k_{eff} is an effective rate constant defined as

$$\frac{1}{k_{eff}} = \left(\frac{1}{k_s a_v} + \frac{1}{k_c a_v} \right)$$

Thus, the length scale over which the acid is consumed in the flow direction is given by

$$l_X \sim \frac{u_{\text{tip}}}{k_{\text{eff}}} \tag{36}$$

In a similar fashion, the length scale l_T in the transverse direction is given by the dispersion-reaction equation

$$D_{eT} \frac{\partial^2 C_f}{\partial y'^2} = k_{\text{eff}} C_f$$

where D_{eT} is the effective transverse dispersion coefficient. The length scale l_T in the transverse direction is given by

$$l_T \sim \sqrt{\frac{D_{eT}}{k_{\text{eff}}}} \tag{37}$$

The ratio of transverse to axial length scales is given by

$$\frac{l_T}{l_X} \sim \frac{\sqrt{k_{\text{eff}} D_{eT}}}{u_{\text{tip}}} = \Lambda \tag{38}$$

The qualitative criteria for different channel shapes in Eqs. 32–34 in terms of parameter Λ are given by $\Lambda \gg O(1)$ for face dissolution, $\Lambda \sim 0.1$ to 1 for wormhole formation and $\Lambda \ll O(1)$ for uniform dissolution. The parameter

$$\Lambda = \frac{\sqrt{\left(\frac{k_c k_s}{k_s + k_c} \right) a_v D_{eT}}}{u_{\text{tip}}} \tag{39}$$

used for determining the conditions for wormhole formation includes the effect of transverse dispersion through D_{eT}, reaction rate constant k_s, pore-scale mass-transfer coefficient k_c, structure-property relations through a_v, effect of convection through velocity u_{tip}, and is independent of domain length L. It should be noted that the above quantities change with time and, thus, Λ provides only an approximate measure for wormhole formation but it is an important parameter to study wormholing. For the case of mass transfer controlled reactions, the parameter reduces to $\Lambda = \sqrt{k_c a_v D_{eT}}/u_{tip}$, while for kinetically controlled reactions it reduces to $\Lambda = \sqrt{k_s a_v D_{eT}}/u_{\text{tip}}$. The optimum injection velocity

$$u_{opt} \sim \sqrt{\left(\frac{k_c k_s}{k_s + k_c} \right) a_v D_{eT}} = \sqrt{k_{eff} D_{eT}} \tag{40}$$

scales as square root of effective rate constant and transverse dispersion coefficient. The parameter Λ in Eq. 39 can be written in terms of dimensionless parameters Damköhler number Da and Peclet number Pe_L as

$$\Lambda = \sqrt{\frac{Da}{Pe_L \left(1 + \frac{\phi^2 r}{Sh} \right)}} (A_v D_T)^{1/2} M \tag{41}$$

$$= \Lambda_o (A_v D_T)^{1/2} M \tag{42}$$

where

$$M = u_o / u_{tip}$$

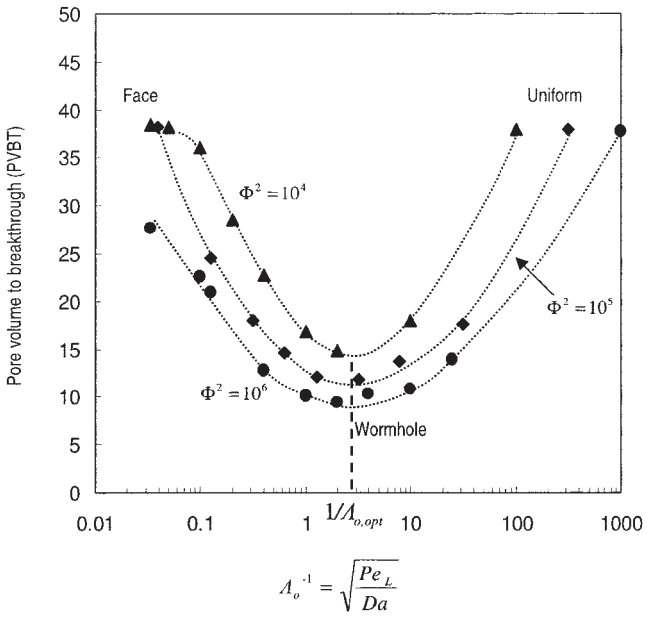

Figure 9. Plot shows pore volume of acid required to breakthrough versus the parameter Λ_o^{-1} for different values of macroscopic Thiele modulus Φ^2.

The reaction is in the kinetic regime ($\phi^2 = 0.07$). Minimum acid volume is required for injection rates where $\Lambda_o \sim O(1)$. This minimum volume of acid required decreases with increasing values of Φ^2.

For clarity, only kinetically controlled reactions ($\phi^2 r/Sh \ll 1$) are analyzed in the remainder of this subsection. The analysis of mass transfer controlled reactions ($\phi^2 r/Sh \gg 1$) is presented in the next section. For kinetically controlled reactions, Λ_o can be reduced to

$$\Lambda_o = \sqrt{\frac{Da}{Pe_L}} = \frac{Da}{\Phi} = \sqrt{\frac{k_s a_o D_m}{u_o^2}} \tag{43}$$

It is observed in the numerical simulations that $\Lambda_o \sim 0.1$ to 1 gives a good first approximation to wormhole formation criterion in Eq. 41. Figure 6 shows the values of Λ_o for different dissolution patterns in the kinetic regime. From the figure it can be seen that wormholing patterns occur at $\Lambda_o = 0.5$ as indicated by the scaling $\Lambda_o \sim O(1)$. For small values of Λ_o ($=0.001$), uniform dissolution is observed and for large values of Λ_o ($=30$), face dissolution is observed. The value of the parameter Λ_o gives an estimate of the optimum injection velocity. The minimum pore volume required for breakthrough, however, depends on the diameter of the wormhole because the volume of acid required to dissolve the material in the wormhole decreases as the wormhole diameter decreases. Since the diameter of the wormhole depends on the thickness of the front l_T in the transverse direction, it is necessary to identify the parameter that controls the transverse front thickness. The parameter that determines the front thickness can be obtained from Eq. 37

$$\frac{l_T}{L} \sim \sqrt{\frac{D_{eT}}{k_{\text{eff}} L^2}} = \frac{\sqrt{\left(1 + \frac{\phi^2 r}{Sh}\right)}}{\Phi} \left(\frac{D_T}{A_v}\right)^{1/2} \tag{44}$$

Again, for kinetically controlled reactions, the above equation reduces to

$$\frac{l_T}{L} \sim \frac{1}{\Phi} \left(\frac{D_T}{A_v}\right)^{1/2} \tag{45}$$

From Eq. 45, it can be seen that the front thickness or the wormhole diameter is inversely proportional to the square root of macroscopic Thiele modulus Φ^2. Thus, for increasing values of macroscopic Thiele modulus (or decreasing levels of dispersion), the diameter of the wormhole decreases, thereby decreasing the minimum pore volume required to breakthrough. Figure 9 shows pore volume of acid required for breakthrough versus reciprocal of the parameter Λ_o for three different values of Φ^2 for a kinetically controlled reaction ($\phi^2 = 0.07$). The minimum pore volume required to breakthrough decreases with increasing values of macroscopic Thiele modulus Φ^2. Figure 10 shows the final porosity profiles at the optimum injection rate in Figure 9 for different values of macroscopic Thiele modulus. It can be seen from the figure that the wormhole diameter decreases with increasing values of Φ^2. The earlier analysis shows that optimum injection rate and minimum pore volume required for breakthrough are determined by Λ_o and macroscopic Thiele modulus Φ^2. The breakthrough curves in Figure 9 are plotted again with respect to Damköhler number Da in Figure 11 for different values of macroscopic Thiele modulus Φ^2. It can be seen from the figure that the optimum Damköhler number is dependent on the value of Φ^2. Thus, changing the value of Φ^2 changes the optimum Damköhler number whereas the parameter Λ is always of order unity for different values of Φ^2 (Figure 9). We believe that Λ gives a better criterion than the optimum Damköhler number for predicting wormhole formation. As shown in Figure 11, Φ^2 does not affect the number of pore volumes required to breakthrough in the high injection rate regime. This is because dispersion effects are negligible at high injection rates, where convection and reaction are the dominant mechanisms. The slope of the breakthrough curve at low injection rates and the minimum pore volume are dependent on the value of Φ^2 showing that dispersion becomes an important mechanism at lower injection rates where wormholing, conical and face dissolution occur. The breakthrough curve for $\Phi^2 = 10^4$ shows a minimum pore volume that is higher than that required for

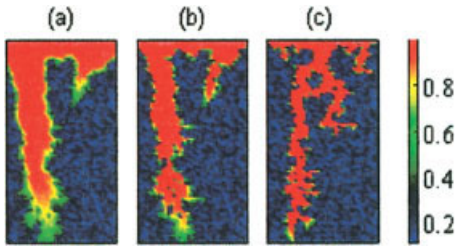

Figure 10. Porosity profiles at the optimum injection rate for the breakthrough curves shown in Figure 9 for different values of Φ^2.

The values of Φ^2 in the figures are: (a) $\Phi^2 = 10^4$ (b) $\Phi^2 = 10^5$ (c) $\Phi^2 = 10^6$. The figures show the effect of macroscopic Thiele modulus Φ^2 on the wormhole diameter. [Color figure can be viewed in the online issue, which is available at http://www.interscience.wiley.com.]

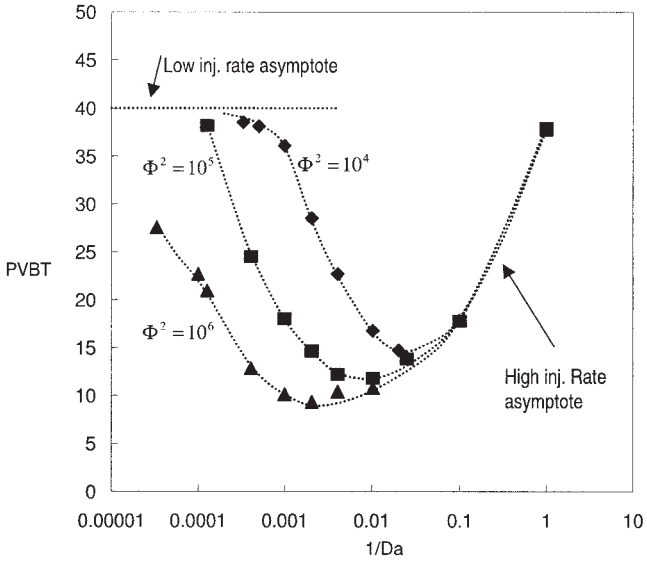

Figure 11. Breakthrough curves in Figure 9 are plotted as function of the reciprocal of Damköhler number.

The figures show that optimum Damköhler number depends on Φ^2. The breakthrough curves are independent of Φ^2 in the high injection rate asymptote because dispersion effects are negligible compared to convection and reaction.

larger values of Φ^2, and it also reaches the low injection rate asymptote at injection rates higher than that required for larger values of Φ^2. This is due to high dispersion level in the system for $\Phi^2 = 10^4$, because of which acid is spread over a larger region at low injection rates, thus, reacting with more material and leading to consumption of more acid. Eventually, all the breakthrough curves for different values of Φ^2 will reach the low injection rate asymptote but the value of injection rate at which they reach the asymptote will depend on the value of Φ^2, or the level of dispersion in the system (Remark: It is observed in the simulations that the effect of axial dispersion on the dissolution patterns is negligible when compared to transverse dispersion. This was verified by suppressing axial and transverse dispersion terms alternatively and comparing it with simulations performed by retaining both axial and transverse dispersion in the model. Transverse dispersion is a growth arresting mechanism in wormhole propagation because it transfers the acid away from the wormhole and therefore prevents fresh acid from reaching the tip of the wormhole.) Figure 11 shows that convection and reaction are dominant mechanisms at high injection rates leading to uniform dissolution, and at very low injection rates transverse dispersion and reaction are the dominant mechanisms leading to face dissolution.

(c) Reaction Regime. The magnitude of $\phi^2 r/Sh$ or k_s/k_c in the denominator of the local equation

$$C_s = \frac{C_f}{\left(1 + \frac{k_s}{k_c}\right)} = \frac{C_f}{\left(1 + \frac{\phi^2 r}{Sh}\right)}$$

determines whether a reaction is in the kinetic or mass transfer controlled regime. In practice, a reaction is considered to be in the kinetic regime if $\phi^2 r/Sh < 0.1$, and in the mass transfer controlled regime if $\phi^2 r/Sh > 10$. For values of $\phi^2 r/Sh$ between 0.1 and 10, a reaction is considered to be in the intermediate regime. The Thiele modulus ϕ^2 is defined with respect to the initial conditions, but the dimensionless pore radius r and Sh change with position and time making the term $\phi^2 r/Sh$ a function of both position and time. At any given time, it is difficult to ascertain whether the reaction in the entire medium is mass transfer or kinetically controlled because these regimes of reaction are defined for a local scale and may not hold true for the entire system. In Table 2, the values of Thiele modulus, the initial values of $\phi^2 r/Sh$ ($r = 1$), and the ratio of interface concentration C_s to fluid phase concentration C_f for different acids used in the experiments of Fredd and Fogler[12] are tabulated for initial pore radii in the range of 1 μm–20 μm. A typical value of 3 is assumed for Sherwood number in the calculations. The ratios of C_s/C_f in the table show that all the acids except HCl are in the kinetic regime during the initial stages of dissolution. The reaction between HCl and calcite is in the intermediate regime. As the reaction proceeds, the pore size increases, thereby increasing the value of $\phi^2 r/Sh$, leading to transitions between different regimes of reaction. To describe these transitions and to capture both the reaction regimes simultaneously, we use two concentration variables in the model.

It has been shown earlier that $\Lambda_o = \sqrt{Da/Pe_L} \sim O(1)$ gives an approximate estimate of the optimal injection conditions for kinetically controlled reactions and the diameter of the wormhole or the pore volume of acid required to breakthrough was observed to depend on the macroscopic Thiele modulus Φ^2. The extensions of these parameters to mass transfer controlled reactions are discussed here. For the case of a mass-transfer controlled reaction ($\phi^2 r/Sh \gg 1$), the species balance Eq. 19 can be reduced to

Table 2. Ratio of Interface to Cup-Mixing Concentration for Different Acids

Acid	D_m (cm^2/s)	k_s (cm/s)	ϕ^2 [r_o = 1 μm–20 μm]	ϕ^2/Sh	C_s/C_f
0.25-M EDTA pH 13	6×10^{-6}	5.3×10^{-5}	0.0017–0.034	0.0006–0.0113	0.99–0.98
0.25-M DTPA pH 4.3	4×10^{-6}	4.8×10^{-5}	0.0024–0.048	0.0008–0.016	0.99–0.98
0.25-M EDTA pH 4	6×10^{-6}	1.4×10^{-4}	0.0046–0.092	0.0015–0.0306	0.99–0.97
0.25-M CDTA pH 4.4	4.5×10^{-6}	2.3×10^{-4}	0.01–0.2	0.003–0.06	0.99–0.94
0.5-M HCl	3.6×10^{-5}	2×10^{-1}	1.11–22.2	0.37–7.4	0.73–0.135

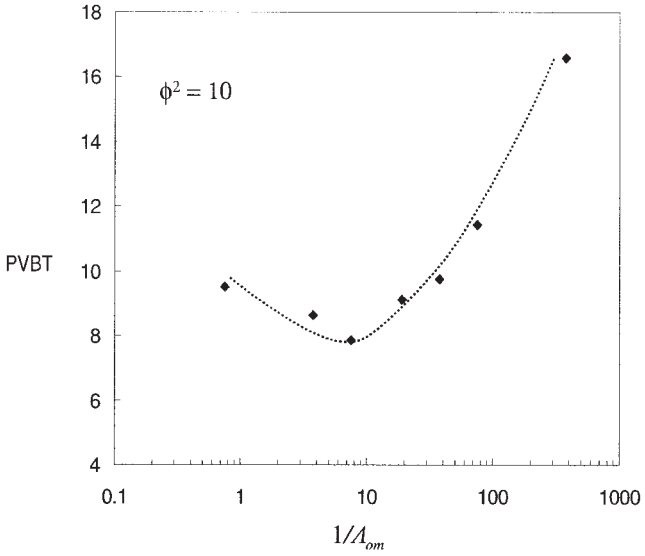

Figure 12. Breakthrough curve of a mass transfer controlled reaction ($\phi^2 = 10$).

The optimum value of Λ_{om} is 0.13. The values of other parameters are $N_{ac} = 0.1$, $\varepsilon_o = 0.2$, $\hat{f} \in [-0.15, 0.15]$, $\Phi_m = 3779$.

$$\frac{\partial(\varepsilon c_f)}{\partial t} + \frac{\partial(u c_f)}{\partial x} + \frac{\partial(v c_f)}{\partial y} = -\frac{P_T Sh A_\nu}{r} c_f + \frac{\partial}{\partial x}\left[\left\{\frac{\alpha_{os}\varepsilon P_T}{\Phi_m^2} + \lambda_x |\mathbf{u}| r\eta\right\}\frac{\partial c_f}{\partial x}\right] + \frac{\partial}{\partial y}\left[\left\{\frac{\alpha_{os}\varepsilon P_T}{\Phi_m^2} + \lambda_y |\mathbf{u}| r\eta\right\}\frac{\partial c_f}{\partial y}\right]$$

where

$$P_T = \frac{a_o L D_m}{2 u_o r_o} \tag{46}$$

is an equivalent to the Damköhler number for mass transfer controlled reactions defined as the ratio of convection time to diffusion time and

$$\Phi_m^2 = P_T Pe_L = \frac{a_o L^2}{2 r_o} \tag{47}$$

is an equivalent to the macroscopic Thiele modulus Φ^2. Note that molecular diffusion or mass transfer coefficients do not appear in the earlier definition because the Peclet number is defined based on molecular diffusion assuming that the main contribution to dispersion is from molecular diffusion. The parameter that determines the optimal injection rate can be derived from Eq. 41, and is given by

$$\Lambda = \sqrt{\frac{P_T}{Pe_L}}\left(\frac{Sh A_\nu D_T}{r}\right)^{1/2} M = \Lambda_{om}\left(\frac{Sh A_\nu D_T}{r}\right)^{1/2} M \tag{48}$$

where

$$\Lambda_{om} = \sqrt{P_T/Pe_L} = \sqrt{\frac{a_o D_m^2}{2 u_o^2 r_o}} \tag{49}$$

From Eq. 44, it can be shown that the minimum pore volume depends on the parameter Φ_m. Equation 48 shows that structure property relations have a stronger influence on the optimal criterion for mass transfer controlled reactions when compared to kinetically controlled reactions where

$$\Lambda = \sqrt{\frac{Da}{Pe_L}}\,(A_\nu D_T)^{1/2} M$$

This result is expected because the mass transfer coefficient is a function of the structure of the porous medium. Figure 12 shows the pore volume of acid required to breakthrough for a mass transfer controlled reaction ($\phi^2 = 10$) as a function of the reciprocal of Λ_{om}. The breakthrough curve shows a minimum at $\Lambda_{om} = 0.13$. However, because of a strong dependence on the structure property relations for mass transfer controlled reactions, the value of Λ_{om} for wormhole formation is expected to be a function of the structure-property relations. The effect of structure-property relations on Λ_{om} is investigated in the following subsection.

Figure 13 shows a comparison of breakthrough curves for kinetic and mass transfer controlled reactions as a function of dimensionless injection rate ϕ^2/Da. Note that this definition of dimensionless injection rate is independent of the reaction rate constant. In the breakthrough curves shown in Figure 13, the effect of reaction regime on breakthrough curves is investigated by changing the reaction rate or pore scale Thiele modulus from a very low ($\phi^2 = 0.001$) to a very large value ($\phi^2 =$

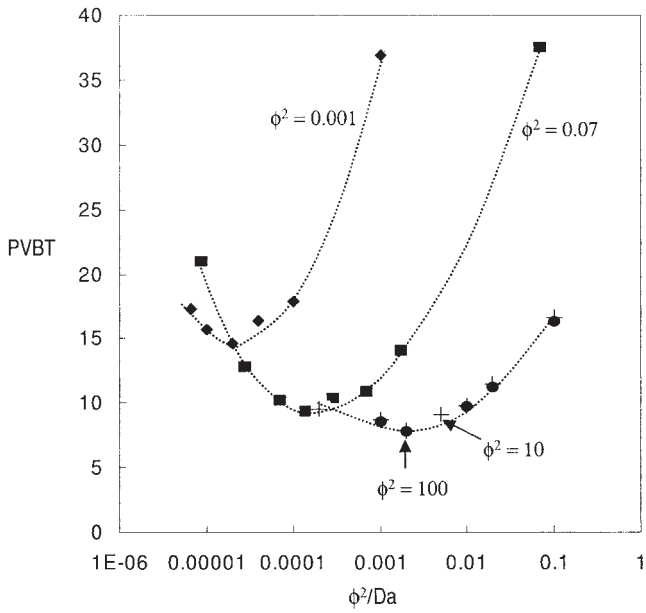

Figure 13. In the plot the reaction rate constant or ϕ^2 is varied to simulate breakthrough curves of kinetic ($\phi^2 = 0.001$, 0.07) and mass transfer ($\phi^2 = 10$, 100) controlled reactions.

The x-coordinate is independent of reaction rate (parameters: $N_{ac} = 0.1$, $\varepsilon_o = 0.2$, $\hat{f} \in [-0.15, 0.15]$).

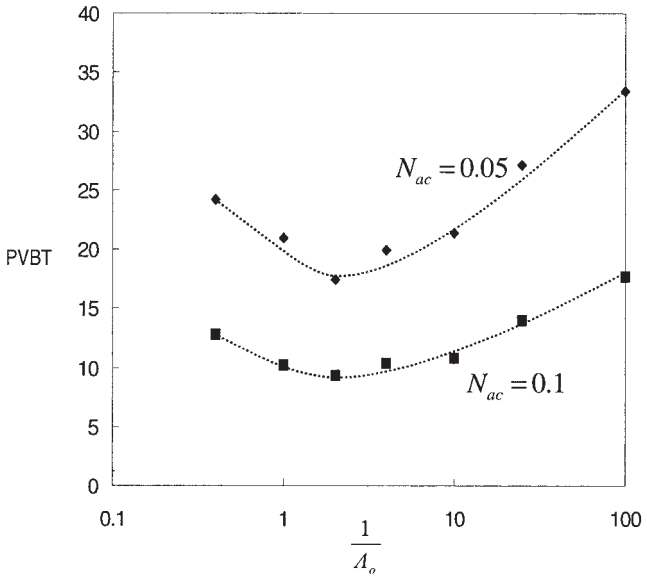

Figure 14. Pore volume required for breakthrough is inversely proportional to the acid capacity number (parameters: $\phi^2 = 0.07$, $\varepsilon_o = 0.2$, $\hat{f} \in [-0.15, 0.15]$, $\Phi = 10^3$).

100), thereby changing the reaction regime from kinetic to mass-transfer control. It could be observed that the optimum injection rate increases with increasing Thiele modulus. Thus, acids like HCl which have a Thiele modulus larger than EDTA should be injected at a higher rate to create wormholes. The minimum volume required to breakthrough the core is observed to be higher for lower values of Thiele modulus. This observation is consistent with experimental data reported in Fredd and Fogler,[12] where the minimum volume required for EDTA is higher than the minimum volume required for HCl to breakthrough the core. It can also be observed from Figure 13 that the injection rate is independent of reaction rate constant for large values of ϕ^2 (see breakthrough curves of $\phi^2 = 10$ and 100), because the system is mass transfer controlled. Figure 13 demonstrates the effect of competition between mass transport and reaction at the pore scale on optimal conditions for injection. Because increasing temperature increases the rate constant a similar behavior as observed in Figure 13 for increasing rate constants is expected when the temperature is increased.

Before closing this section, we consider briefly the role of heterogeneity length scale ($l = L_h/2r_o$) on wormhole formation. In all the simulations presented in this work, we have taken L_h to be the grid size (which in physical units is 1 mm). In practice, this length scale in carbonates can vary from the pore size to the core size. It may be seen intuitively that when $L_h \ll l_T$ and l_X the structure of the wormholes is not influenced by L_h, as transverse dispersion dominates over the small length scales. Similarly, when $L_h \gg l_T$ and l_X, wormhole formation is again not influenced by L_h, as it is a local phenomenon now dictated by dispersion and reaction at smaller scales. Thus, we expect the heterogeneity length scale to play a role in determining the wormhole structure only when L_h is of the same order of magnitude as the dispersion-reaction (l_T), and convection-reaction (l_X) length scales. Quantitative determination of this effect requires us to consider extremely fine grids, which is beyond the scope of this work.

(d) Acid Capacity Number. The acid capacity number N_{ac} ($=\alpha C_o/\rho_s$) depends on the inlet concentration of the acid. Figure 14 shows the breakthrough curves for acid capacity numbers of 0.05 and 0.1. From the breakthrough curves it can be seen that the minimum shifts proportionally with the acid capacity number. For low values of acid capacity number ($N_{ac} \ll 1$), the time scale over which porosity changes significantly is much larger than the time scale associated with changes in concentration. In such a situation, a pseudo-steady-state approximation can be made and Eqs. 19 and 20 can be reduced to

$$u\frac{\partial c_f}{\partial x} + \nu\frac{\partial c_f}{\partial y} = -\frac{DaA_\nu c_f}{\left(1+\frac{\phi^2 r}{Sh}\right)} + \frac{\partial}{\partial x}\left[\left\{\frac{\alpha_{os}\varepsilon Da}{\Phi^2} + \lambda_x|\mathbf{u}|r\eta\right\}\frac{\partial c_f}{\partial x}\right] + \frac{\partial}{\partial y}\left[\left\{\frac{\alpha_{os}\varepsilon Da}{\Phi^2} + \lambda_y|\mathbf{u}|r\eta\right\}\frac{\partial c_f}{\partial y}\right] \quad (50)$$

and

$$\frac{\partial \varepsilon}{\partial \tau} = \frac{DaA_\nu c_f}{\left(1+\frac{\phi^2 r}{Sh}\right)} \quad (51)$$

where $\tau = N_{ac}t$. Since the earlier equations are independent of N_{ac}, the breakthrough time τ_{BT} is independent of N_{ac}. The breakthrough volume, defined as $t/\varepsilon_o = \tau_{BT}/N_{ac}\varepsilon_o$, is, therefore, inversely proportional to acid capacity number at low values of N_{ac} as demonstrated in Figure 14.

(e) Effect of Structure-Property Relations. In the previous subsections, the effect of heterogeneity, injection conditions, reaction regime and acid concentration on wormhole formation were investigated using the structure-property relations given by Eqs. 7–9. It has been observed that the optimum injection rate and breakthrough volume are governed by parameters Λ_o and Φ^2 for kinetically controlled reactions and Λ_{om} and Φ_m^2 for mass transfer controlled reactions for a given set of structure-property relations. In this subsection, the effect of structure-property relations on the optimal conditions is investigated using a different correlation given by

$$\frac{K}{K_o} = \left(\frac{\varepsilon}{\varepsilon_o}\right)^3 \exp\left[b\left(\frac{\varepsilon-\varepsilon_o}{1-\varepsilon}\right)\right] \quad (52)$$

The relations for average pore radius and interfacial area are given by Eqs. 8 and 9. By changing the value of b in Eq. 52, the increase in local permeability with porosity can be made gradual or steep. Figures 15 and 16 show the effect of b on evolution of permeability and interfacial area with porosity. It can be seen from the figures that for low values of b, the changes in permeability and interfacial area with porosity are gradual until the value of local porosity is close to unity, and the change is very steep for large values of b. Figure 17 shows the effect of structure property relations on the breakthrough curve for very low and large values of b. A mass transfer controlled reaction is considered in these simulations because the effect of structure property relations on optimal conditions

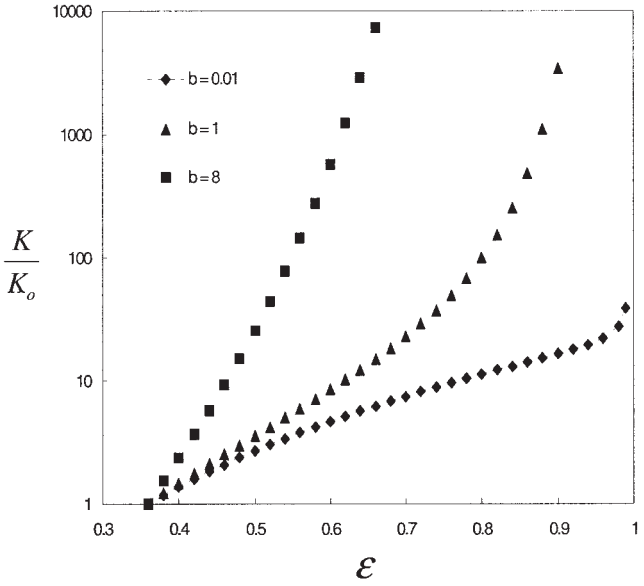

Figure 15. Evolution of permeability with porosity for different values of *b*.

The initial value of porosity ε_o is equal to 0.36.

is significant for mass-transfer controlled reactions as discussed earlier. It can be seen that the optimum Λ_{om}, although different for different structure property relations is approximately order unity for large changes in the qualitative behavior of structure-property relations. The value of minimum pore volume to breakthrough is also observed to depend on the structure-property relations. The lower value of minimum pore volume for a large value of b or a steep change in evolution of permeability is because of a rapid increase in adverse mobility ratio between the dissolved and undissolved medium at the

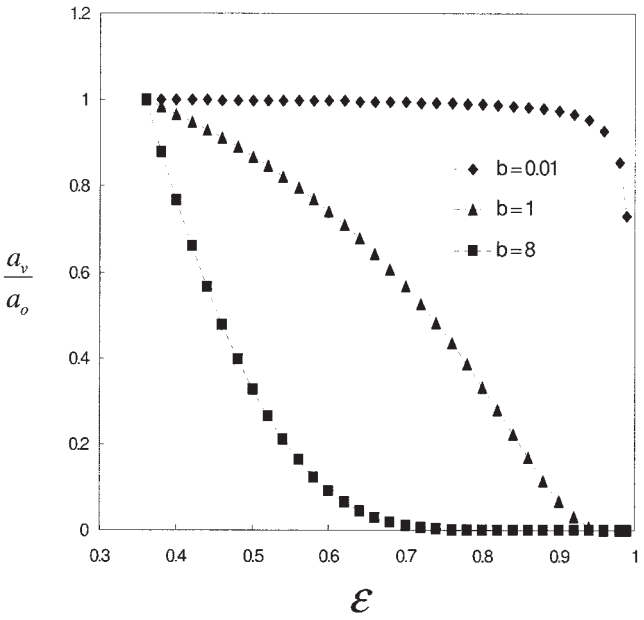

Figure 16. The change in interfacial area is very gradual for low values of *b* and steep for large values of *b*.

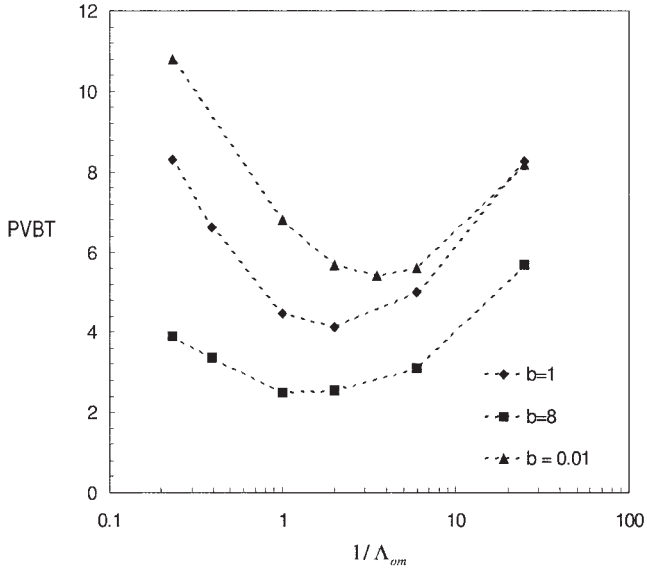

Figure 17. The effect of structure-property relations on breakthrough volume is shown in the figure by varying the value of *b*.

For low values of b the evolution of permeability and interfacial area are gradual and the evolution is steep for large values of b. The parameters used in the simulation are $\varepsilon_o = 0.36$, $\hat{f} \in [-0.03, 0.03]$, $\phi^2 = 50$, $\Phi_m = 534$, $\alpha_o = 0.2$.

reaction front. This leads to faster development and propagation of wormholes leading to shorter breakthrough times or lower pore volumes to breakthrough.

Experimental Comparison

Wormholing in carbonates is a 3-D phenomenon. Comparison of model predictions with experimental data requires a 3-D model. Since the current model is 2-D, and due to a lack of 2-D experimental data in carbonates, the model predictions are compared to 2-D experiments on salt-packs reported in Golfier et al.[26] In those experiments, undersaturated salt solution was injected into solid salt packed in a Hele-Shaw cell of dimensions 25 cm in length, 5 cm in width, and 1 mm in thickness. Because the thickness of the cell is very small compared to the width and the length of the cell, this configuration may be considered 2-D (provided the wormhole diameter is bigger than the thickness, which is the case in these experiments). The average values of permeability and porosity of the salt-packs used in the experiments are reported to be 1.5×10^{-11} m^2 and 0.36, respectively. Solid salt dissolves in the undersaturated salt solution, and creates dissolution patterns that are very similar to patterns observed in carbonates. The dissolution of salt is assumed to be a mass transfer controlled process (Remark: This assumption breaks down as the salt concentration in the injected solution approaches saturation value). Figure 18 shows the experimental data on pore volumes of salt solution required to breakthrough at different injection rates for two different inlet concentrations (150 g/L and 230 g/L) of salt solution. The saturation concentration (C_{sat}) of salt is 360 g/L and the density of salt (ρ_{salt}) is 2.16 g/cm^3. The dissolution of salt in an undersaturated salt solution is a process very similar to dissolution of carbonate due to reaction with

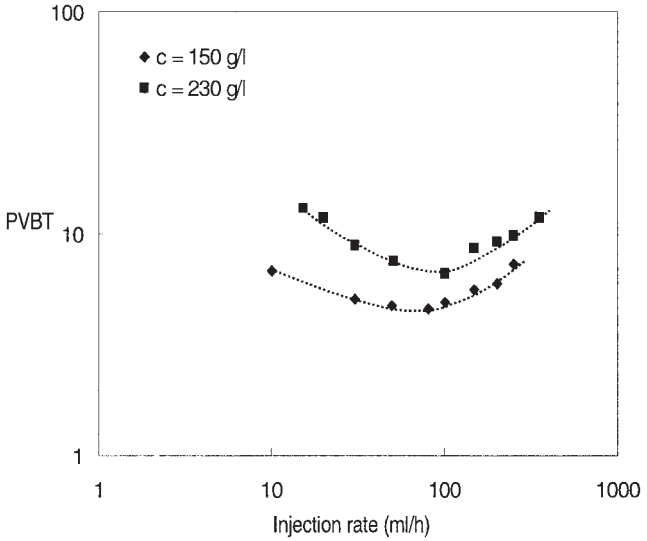

Figure 18. Experimental data on salt dissolution reported in Golfier et al.[26]

Under-saturated salt solution was injected into a salt-pack to create dissolution patterns. The breakthrough curves in the plot correspond to two different inlet concentrations, 150 g/L and 230 g/L, of salt solution.

acid, and the model developed here can be used for salt dissolution by defining the acid concentration to be $C_f = C_{sat} - C_{salt}$. Thus, the acid capacity number for a salt solution of concentration C_o g/L is given by

$$N_{ac} = \frac{C_{sat} - C_o}{\rho_{\text{salt}}}$$

Using the above equation, the acid capacity numbers for salt concentrations of 230 g/L and 150 g/L are calculated to be 0.06 and 0.097 respectively.

To compare model predictions with experimental data, we need information on initial average pore radius, interfacial area, and structure-property relations. This data is difficult to obtain directly and, hence, the model is calibrated with experimental data to obtain these parameters. Using these parameters, the model is simulated for a different set of experimental data for comparison. From the earlier results, we know that for mass-transfer controlled reactions, the pore volumes of salt solution required to breakthrough is a function of the parameters Λ_{om}, Φ_m^2, and structure property relations for a given inlet concentration. The model is first calibrated to the breakthrough curve corresponding to the inlet salt solution concentration of 150 g/L. For calibration, the largest uncertainty arises from lack of information on structure-property relations, so the relation in Eq. 52 is used with the value of $b = 1$. The minimum pore volume to breakthrough depends on Φ_m^2, and its value is used to calibrate to the experimental minimum after the structure property relations are fixed. Then, the pore volume to breakthrough curve is generated for different values of Λ_{om}. Figure 19 shows the calibration curve of the model with the experimental data. The value of Φ_m used for calibration is 534. This value of Φ_m is used to simulate the model for inlet salt concentration of 230 g/L ($N_{ac} = 0.06$). The comparison of

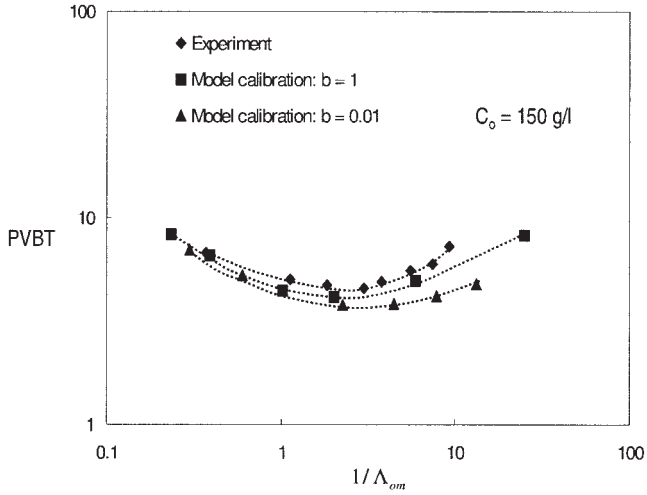

Figure 19. Plot shows the calibration of the model with experimental data for different structure-property relations.

model predictions with experimental data is shown in Figure 20. The value of a_o/r_o can be calculated using Eq. 47, and is found to be 912.49 cm^{-2}. Using this value of a_o/r_o, and the optimum value $\Lambda_{om} = 0.33$, the value of injection velocity is calculated from Eq. 49 to be 1.29×10^{-3} cm/s ($D_m = 2 \times 10^{-5}$ cm^2/s). This value is much lower when compared to the experimental optimum injection velocity $u_o = 0.045$ cm/s. To get a better estimate of the injection velocity a different value of $b = 0.01$ is used for the structure-property relations, and the model is calibrated with the data for inlet salt concentration of 150 g/L (see Figure 19). The value of Φ_m used for calibration is 1,195. The model predictions for this value of b for inlet salt solution concentration of 230 g/L is shown in Figure 20. The injection velocity is calculated using the procedure described before and is found to be 3×10^{-3} cm/s. (One possible reason for this calculated value to be one order of magnitude smaller than the experimental value is our assumption of a constant

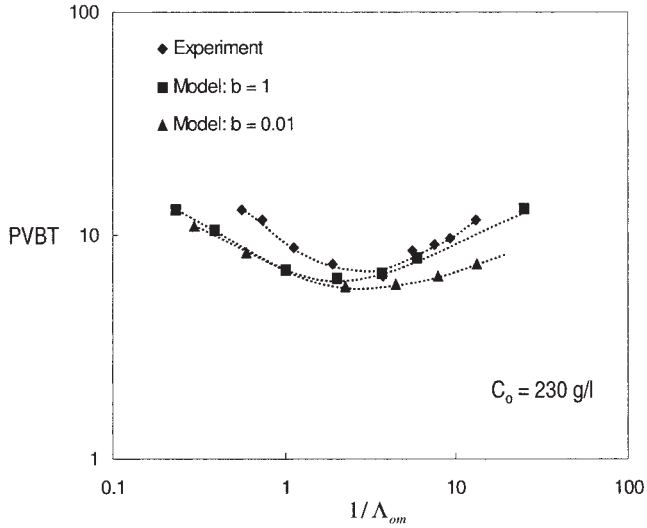

Figure 20. Model predictions with experimental data for different structure-property relations.

α_{os}. In general, dissolution increases the connectivity between the pores and, hence, the effective transverse dispersion coefficient. Thus, if we include the variation of the transverse dispersion coefficient also in the structure-property relations, it follows from Eq. 48 that the calculated u_o will be higher.)

The earlier comparisons show that the model predictions in terms of pore volume are in reasonable agreement with experimental data. However, the predictions of injection velocity are not in good agreement with experimental values due to lack of information on structure-property relations. Further investigation on obtaining structure-property relations and calibration methods are required for experimental comparison.

Conclusions and Discussion

The main contribution of this work is the development of a two-scale continuum model that retains the qualitative features of reactive dissolution of porous media. We have also analyzed in detail the 2-D version of the model and determined the influence of various parameters such as the level of dispersion, the magnitude of heterogeneities, strength of acid, and pore scale mass transfer on wormhole formation. It is observed that wormhole formation depends on the magnitude of convection, dispersion and reaction effects in the system. A qualitative criterion is developed to predict conditions required for creating wormholes and it is given by $\Lambda \sim O(1)$, where $\Lambda = \sqrt{k_{eff} D_{eT}}/u_o$. The branched wormholes observed in experiments are found to be a result of the heterogeneities in the core. The optimum injection rate and minimum volume required to breakthrough were found to be weak functions of initial heterogeneity in the core. Pore-scale mass transfer and reaction were observed to have a strong influence on the optimal conditions. The model predictions are in qualitative agreement with laboratory data on carbonate cores and salt-packs presented in the literature.

The model presented here as well as the numerical calculations can be extended in several ways. Our preliminary calculations indicated that the fractal dimension of the wormhole formed depends both on the magnitude of heterogeneity and the rate constant (ϕ^2). Strong acids such as HCl and higher levels of heterogeneities produce thinner wormholes but have a higher fractal dimension. In contrast, weak acids and lower levels of heterogeneities lead to fatter wormholes having lower fractal dimension. It is not clear intuitively which of these is preferred because in the former case, the interfacial area between the wormhole, and the reservoir rock is higher while in the latter case, the permeability of the wormhole is larger. The model presented here can be used to quantify the effect of wormholes of different fractal dimension and size on the overall permeability.

The calculations presented in this work were limited to the case of linear kinetics and constant physical properties of the fluid. The model can be extended to include multistep chemistry at the pore scale as well as changing physical properties (for example, viscosity varying with local pH) on wormhole structure. Likewise, all the calculations presented here are for a fixed aspect ratio. The model can be used to determine the density of wormholes by changing the aspect ratio corresponding to that near a wellbore (for example, height of domain much larger than width). Preliminary calculations of this type were presented by Panga et al.[22] These calculations, as well as additional simulations using a 3-D version of the model will be pursued in future work.

Acknowledgments

This work was partially supported by an unrestricted grant by Schlumberger to the University of Houston. We thank Drs. Eduard Siebrits and Philippe Tardy for many helpful comments.

Literature Cited

1. William B, Gidley J, Schechter RS. Acidizing Fundamentals. SPE Monograph Series; 1992.
2. Schechter RS. Oil Well Stimulation. New Jersey: Prentice Hall Inc.; 1992.
3. Economides M, Hill A, Ehlig-Economides C. Petroleum Production Systems. Prentice Hall Inc.; 1993.
4. Economides M., Nolte K (Eds.). *Reservoir Stimulation.* Wiley; 2000.
5. Daccord G, Lenormand R. Fractal patterns from chemical dissolution. *Nature.* 1987; 325: 41–43.
6. Daccord G. Chemical dissolution of a porous medium by a reactive fluid. *Phys Rev Lett.* 1987; 58: 479–482.
7. Daccord G, Lenormand R, Lietard O. Chemical dissolution of a porous medium by a reactive fluid-1: model for the "wormholing." *Chem Eng Sci.* 1993a; 48: 169–178.
8. Daccord G, Lenormand R, Lietard O. Chemical dissolution of a porous medium by a reactive fluid-2: convection vs reaction, behavior diagram. *Chem Eng Sci.* 1993b; 48: 179–188.
9. Hoefner ML, Fogler HS. Pore evolution and channel formation during flow and reaction in porous media. *AIChE J.* 1988; 34: 45–54.
10. Wang Y, Hill AD, Schechter RS. The optimum injection rate for matrix acidizing of carbonate formations. *SPE 26578. SPE Ann. Tech. Conf. and Exhib., Houston, TX;* 1993; 675–687.
11. Frick TP, Mostofizadeh B, Economides MJ. Analysis of radial core experiments of hydrochloric acid interaction with limestones. *SPE 27402. SPE Intl. Symposium on Formation Damage Control, Lafayette, LA*; 1994;577–592.
12. Fredd CN, Fogler HS. Influence of transport and reaction on wormhole formation in carbonate porous media. *AIChE J.* 1998; 44: 1933–1949.
13. Bazin B. From matrix acidizing to acid fracturing: A laboratory evaluation of acid/rock interactions. SPE Prod. & Facilities. Feb. 2001; 22–29.
14. Buijse MA. Understanding wormholing mechanisms can improve acid treatments in carbonate formations. SPE Prod. & Facilities. Aug. 2000; 168.
15. Fredd CN, Fogler HS. Optimum conditions for wormhole formation in carbonate porous media: Influence of transport and reaction. *SPE J.* 1999; 4: 196.
16. Fredd CN. Dynamic model of wormhole formation demonstrates conditions for effective skin reduction during carbonate matrix acidizing. *SPE 59537. SPE Permian Basin Oil and Gas Recovery Conference.* Midland, Texas; 2000: 1.
17. Daccord G, Touboul E, Lenormand R. Carbonate Acidizing: Toward a quantitative model of the wormholing phenomenon. *SPE Prod Eng.* 1989; 63.
18. Hung KM, Hill AD, Sepehrnoori K. A mechanistic model of wormhole growth in carbonate matrix acidizing and acid fracturing. *J Pet Tech.* 1989; 41: 59.
19. Huang T, Hill AD, Schechter RS. Reaction rate and fluid loss: The keys to wormhole initiation and propagation in carbonate acidizing. SPE 37312. SPE Intl. Symposium on Oilfield Chemistry, Houston, Texas 1997; 775.
20. Huang T, Zhu D, Hill AD. Prediction of wormhole population density in carbonate matrix acidizing. SPE 54723. SPE European Formation Damage Conference; 1999;1 The Hague, Netherlands.
21. Gdanski R. A fundamentally new model of acid wormholing in carbonates. SPE 54719. SPE European Formation Damage Conference; 1999: 1 The Hague, Netherlands.
22. Panga MKR, Ziauddin M, Gandikota R, Balakotaiah V. A new model for predicting wormhole structure and formation in acid stimulation of carbonates. SPE 86517. SPE International Symposium and Exhibition on Formation Damage Control; 2004;1 Lafayette, Louisiana.
23. Liu, X, Ormond A, Bartko K, Li Y, Ortoleva P. A geochemical

reaction-transport simulator for matrix acidizing analysis and design. *J Pet Sci Eng.* 1996; 181.
24. Chen Y, Mu J, Chen W, Davis D, Ortoleva P. Optimizing matrix acidizing for near-borehole remediation using the CIRF reaction-transport simulator. SPE 26184. SPE Gas Tech. Symposium. Calgary, Alberta; 1993; 471.
25. Chen Y, Fambrough J, Bartko K, Li Y, Montgomery C, Ortoleva P. Reaction-Transport simulation of matrix acidizing and optimal acidizing strategies. SPE 37282. SPE International Symposium on Oilfield Chemistry. Houston, Texas 1997; 679.
26. Golfier F, Zarcone C, Bazin B, Lenormand R, Lasseux D, Quintard M. On the ability of a Darcy-scale model to capture wormhole formation during the dissolution of a porous medium. *J Fluid Mech.* 2002; 457: 213.
27. Froment GF, Bischoff KB. Chemical Reactor Analysis and Design. John Wiley & Sons, 1990.
28. Chadam J, Hoff D, Merino E, Ortoleva P, Sen A. Reactive infiltration instabilities. *IMA J Appl Math.* 1986; 36: 207.
29. Sherwood JD. Stability of a plane reaction front in a porous medium. *Chem Eng Sci.* 1987; 42: 1823.
30. Hinch EJ, Bhatt BS. Stability of an acid front moving through porous rock. *J Fluid Mech.* 1990; 212: 279.
31. Crompton S, Grindrod P. A geometric approach to fingering instabilities for reaction fronts in fully coupled geochemical systems. *IMA J Appl. Math.* 1996; 57: 29.
32. Homsy GM. Viscous fingering in porous media. *Ann Rev Fluid Mech.* 1987; 19: 271.
33. Gupta N, Balakotaiah V. Heat and mass transfer coefficients in catalytic monoliths. *Chem Eng Sci.* 2001; 56: 4771.
34. Balakotaiah V, West DH. Shape normalization and analysis of the mass transfer controlled regime in catalytic monoliths. *Chem Eng Sci.* 2002; 57: 1269.

Appendix A

Numerical algorithm

The equations are discretized on a 2-D domain using a control volume approach. While discretizing the species balance equation, an upwind scheme is used for the convective terms in the equation. The following algorithm is used to simulate flow and reaction in the medium. The pressure, concentration and porosity profiles in the domain at time t are denoted by p_t, c_t and ε_t. Porosity and concentration profiles in the domain are obtained for time $t + \Delta t$ ($c_{t+\Delta t}$, $\varepsilon_{t+\Delta t}$), by integrating the species balance and porosity evolution equations simultaneously using the flow field calculated from the pressure profile (p_t) by applying Darcy's law. Integration of concentration and porosity profiles is performed using Gear's method for initial value problems. The calculation for concentration and porosity profiles is then repeated for time $t_{half} = t + \Delta t/2$ using the velocity profile at time t. The flow field at $t + \Delta t/2$ is then calculated using the concentration profile c_{half} and porosity profile ε_{half}. Using the flow profile at t_{half} the values of concentration and porosity are again calculated for time $t + \Delta t$, and are denoted by c_{new} and ε_{new}. To ensure convergence, the norms $|c_{t+\Delta t} - c_{new}|$ and $|\varepsilon_{t+\Delta t} - \varepsilon_{new}|$ are maintained below a set tolerance. If the tolerance criterion is not satisfied the calculations are repeated for a smaller time step. The earlier procedure is repeated until the breakthrough of the acid which is defined as the decrease in the initial pressure by a factor 100.

Manuscript received Feb. 16, 2005, and revision received Apr. 25, 2005.